Platinum on Nanodiamond: A Promising Prodrug Conjugated with Stealth Polyglycerol, Targeting Peptide and Acid-Responsive Antitumor Drug

Li Zhao, Yong-Hong Xu, Hongmei Qin, Shigeaki Abe, Tsukasa Akasaka, Tokuhiro Chano, Fumio Watari, Takahide Kimura, Naoki Komatsu and Xiao Chen**

In the field of nanomedicine, nanoparticles with various functions are required for in vivo applications such as biomedical imaging and drug delivery. Therefore, chemical functionalization of nanoparticles has been extensively investigated. Herein, nanodiamond (ND) coated with polyglycerol (PG) and its derivatives is reported to impart good solubility in a physiological environment, a stealth nature to avoid nonspecific uptake, a targeting property to be taken up by a specific cell, and an acid-responsive drug release property to kill cancer cells. ND is first grafted with PG and the resulting ND-PG has a high solubility in physiological media. Since a large number of hydroxyl groups in PG provide scaffolds for further surface functionalization, the targeting RGD peptide and Pt-based drug are immobilized to give ND-PG-RGD, ND-PG-Pt and ND-PG-RGD-Pt. The ND with intrinsic fluorescence is also functionalized by PG and RGD to confirm cellular uptake and intracellular localization fluorescently. The results of the cell experiments indicate that PG coating shielded fND from the uptake by HeLa and U87MG cells. In contrast, fND-PG-RGD is taken up by U87MG, not HeLa cells, exhibiting high targeting efficacy. When ND-PG-RGD-Pt is applied, U87MG is selectively killed against HeLa. The multi-functional ND is a promising prodrug in targeting chemotherapy.

1. Introduction

Nanomedicine has been attracting growing interest from a viewpoint of fundamental science as well as clinical medicine.[1–5] The central subjects in nanomedicine are biomedical imaging for diagnosis and drug delivery for therapy by use of nanoparticle.[6–12] In both purposes, the nanoparticles should be accumulated in the specific lesion as much as possible.[13] Therefore, the nanoparticles have been designed so far to have maximal targeting and stealth nature simultaneously.[14–16] The fundamental techniques to control the particle size and the surface functionality of nanoparticles have been extensively studied in view of good solubility and stability with anti-biofouling property, passive and active targeting features, and prolonged circulation time in vivo.[17,18] Although polyethylene glycol (PEG) has been considered to be the most effective surface functionality, especially, due to the stealth nature, recent studies reported its disadvantages, designated as "PEG dilemma", such as immune response and interference with cellular uptake.[19] In this context, it is proposed that polyglycerol (PG)[20] is a better alternative to PEG for biomedical applications of nanoparticle[21] in terms of biocompatibility, solubility and stability in physiological environment, and extensibility for further chemical derivatization.[22–28] PG is also reported to be more resistive towards protein adsorption than PEG, exhibiting better stealth effect from mononuclear phagocyte system.[19,29,30] To take advantage of the above characteristics of PG, PG-coating has been extensively applied quite recently to nanoparticles such as superparamagnetic iron oxide nanoparticle,[25,31,32] silica-encapsulated iron oxide nanoparticle,[33] nanodiamond (ND),[24,34–36] zinc oxide nanoparticle,[26] carbon nanotubes,[37–40] quantum dots,[41] Fe@Au nanoparticles[42] and mesoporous silica nanoparticles,[43] and even stem cell.[44] In view of the application as a drug carrier, however, more functionalities are required such as high targeting efficiency and controlled drug release,[33,43] prompting us to develop multi-functional ND-PG with targeting peptide and acid-responsive Pt-based drug as well as intrinsic fluorescence from the ND core.[45,46]

Dr. L. Zhao, Dr. H. Qin, Prof. T. Kimura, Prof. N. Komatsu
Department of Chemistry
Shiga University of Medical Science, Seta
Otsu 520–2192, Japan
E-mail: nkomatsu@belle.shiga-med.ac.jp
Dr. Y.-H. Xu
Institute of Ophthalmological Research
Department of Ophthalmology
Renmin Hospital of Wuhan University
Wuhan 430060, China
Dr. S. Abe, Dr. T. Akasaka, Prof. F. Watari, Dr. X. Chen
Department of Biomedical
Dental Materials and Engineering
Graduate School of Dental Medicine
Hokkaido University
Sapporo 060–8586, Japan
E-mail: mornsmile@yahoo.com
Prof. T. Chano
Department of Clinical Laboratory Medicine
Shiga University of Medical Science
Seta, Otsu 520–2192, Japan

DOI: 10.1002/adfm.201304298

On the other hand, ND is one of the ideal nanoparticles in nanomedicine[47,48] due to its high biocompatibility, high extensibility of the surface functionality, and intrinsic non-bleaching and non-blinking fluorescence.[46,49] Therefore, ND has been used recently for cell labeling,[50,51] in vivo imaging[52] and drug delivery.[53–57] Behind these excellent applications, fundamental technique to impart good solubility to ND in physiological environment has been still investigated by PG functionalization mentioned above,[24,34] protein coating[58] and silica encapsulation.[59] Herein, we report on synthesis, characterization, and in vitro evaluation of ND-PG based prodrug having sufficient solubility in physiological environment, clear stealth nature avoiding nonspecific cellular uptake, good targeting efficacy by the conjugated peptide and acid-responsive nature in the release of the Pt(II)-based drug.

2. Results and Discussion

2.1. Synthesis and Characterization of ND-PG Conjugated with Targeting Peptide and Pt-Based Drug

ND powder, kindly provided by Tomei Diamond Co., is prepared from bulk diamonds synthesized by a static high pressure high temperature (HPHT) method. Among various sizes, we chose ND with 50 nm size (ND50) for this study in view of enhanced permeation and retention (EPR) effect in cancer therapy.[18,60] The ND50 was covalently functionalized with hyperbranched PG through ring-opening polymerization of glycidol according to the procedure we reported previously.[24] The resulting ND50-PG showed very good solubility (≥20 mg/mL) and stability in water; only a few or no precipitates were found in the solution with concentration of 20 mg/mL over three months. In addition, PG contains a large number of hydroxyl groups which can be utilized for further surface functionalization to add more functions.

To conjugate with a targeting peptide and load an anticancer drug, ND50-PG was engineered as shown in **Scheme 1**. After some of the hydroxyl groups of ND50-PG were reacted with tosyl chloride (TsCl), the resulting tosylates (ND-PG-OTs) were substituted by azido groups (ND-PG-N_3).[25,35,36] Carboxyl groups were introduced in ND-PG-N_3 as ligands for the Pt-based drug by nucleophilic ring-opening of succinic anhydride at the hydroxyl groups.[43,61] The resulting ND-PG-N_3-COOH was conjugated with RGD peptide through click chemistry of the azido groups with the propiolic amide of RGD peptide, yielding ND-PG-RGD-COOH.[25] Finally, *cis*-$(NH_3)_2$Pt(II) moiety was immobilized on the ND-PG-RGD-COOH through ligand exchange of Cl^- at the cisplatin with $-COO^-$ under a slightly basic condition, affording ND-PG-RGD-Pt (Scheme 1).[43,61] ND-PG-Pt without RGD peptide was also prepared as a control from ND-PG-COOH.

All the ND-based materials shown in Scheme 1 were characterized by FTIR (**Figure 1**).[25,35,36] The absorption bands at 1350 and 1176 cm^{-1} are attributed to asymmetric and symmetric stretchings of S→O bonds of the tosyl group in ND-PG-OTs, respectively (Figure 1B). The ND-PG-N_3 clearly showed a characteristic strong absorption band at 2100 cm^{-1} corresponding to azido group (Figure 1C). The absorption band at 1730 cm^{-1} is assigned to C=O stretching of carboxylic acid in ND-PG-N_3-COOH (Figure 1D).[61] The azido absorption band disappeared after the click conjugation of the targeting peptide (Figure 1E), indicating the complete consumption of azido groups. The immobilization of RGD peptide was verified by the absorption bands at 1650 and 1590 cm^{-1}, which correspond to the C=O stretching and N-H bending of amide bonds in the peptide, respectively.[25] After the drug loading, the absorption band of carboxylic acid was partially consumed to give a new band at 1570 cm^{-1} attributed to C=O stretching of carboxylate (Figure 1F) which coordinated with the Pt(II).

Although IR spectra (Figure 1) gave us valuable information to identify the chemical structures of the ND50-PG derivatives mentioned above, more evidence is highly desired for more strict identification. Therefore, we further characterized the ND50-PG derivatives by ^{1}H- and ^{13}C-NMR in a solution phase. Owing to the good aqueous solubility (≥20 mg/mL) of

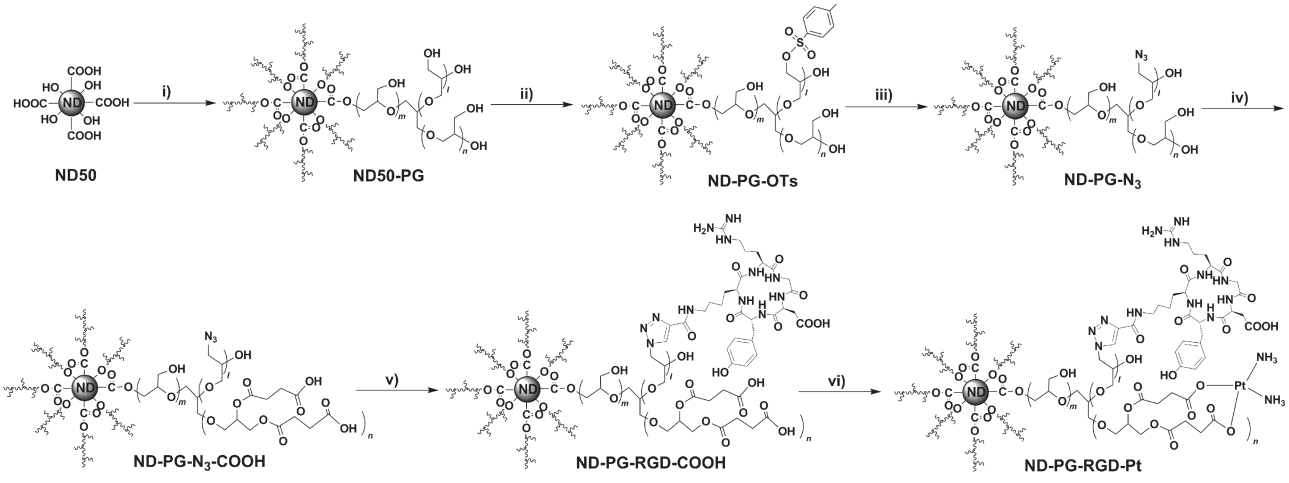

Scheme 1. Surface engineering on ND50-PG for conjugation with RGD peptide and Pt(II)-based drug. i) glycidol, 140 °C, 20 h; ii) *p*-TsCl, pyridine, 0 °C ~ r. t., overnight; iii) NaN_3, 90 °C, overnight; iv) succinic anhydride, DMAP, pyridine, 0 °C ~ r. t., overnight; v) RGD propargyl amide, copper(II) sulfate pentahydrate, sodium ascorbate, r. t., 48 h; vi) cisplatin, 0.5 M NaOH, pH 8.0, r. t., 72 h.

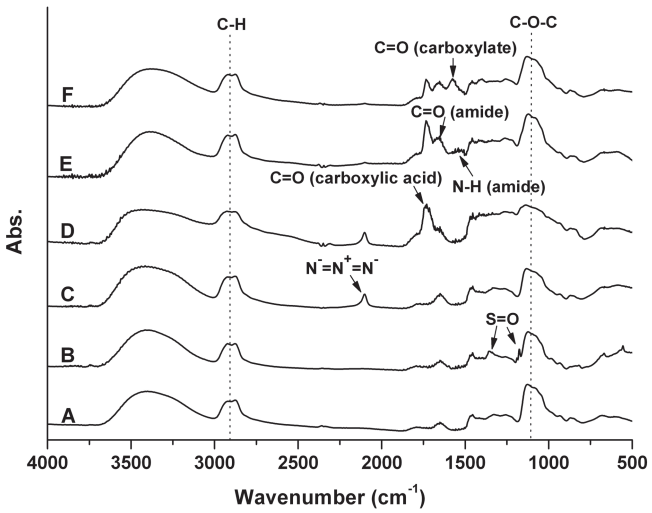

Figure 1. FTIR spectra of A) ND50-PG, B) ND-PG-OTs, C) ND-PG-N_3, D) ND-PG-N_3-COOH, E) ND-PG-RGD-COOH, and F) ND-PG-RGD-Pt. Arrows indicate new absorption bands in each step.

ND50-PG, its derivatives shown in Scheme 1 also possessed enough solubility for NMR measurements even though hydrophobic functionality such as tosylate was bound.

In the ^{1}H-NMR spectra shown in **Figure 2**B,[35,36] the aromatic and methyl hydrogens at the tosyl group are observed at 7.7 and 7.4 ppm, and 2.3 ppm in addition to the PG hydrogens at 3.6 ppm. Since only S→O functionality was characterized on the IR (Figure 1B), the ^{1}H-NMR spectrum (Figure 2B) complements the IR in the characterization of ND-PG-OTs. After the reaction of ND-PG-OTs with sodium azide, the peaks from the tosyl group disappeared in Figure 2C, indicating the complete substitution of the tosyl group. The shoulder appeared at ca. 3.4 ppm is assigned to the methylene hydrogens adjacent to azido groups of the ND-PG-N_3,[36,62] indicating the nucleophilic substitution of tosylate by azido. Introduction of carboxyl groups

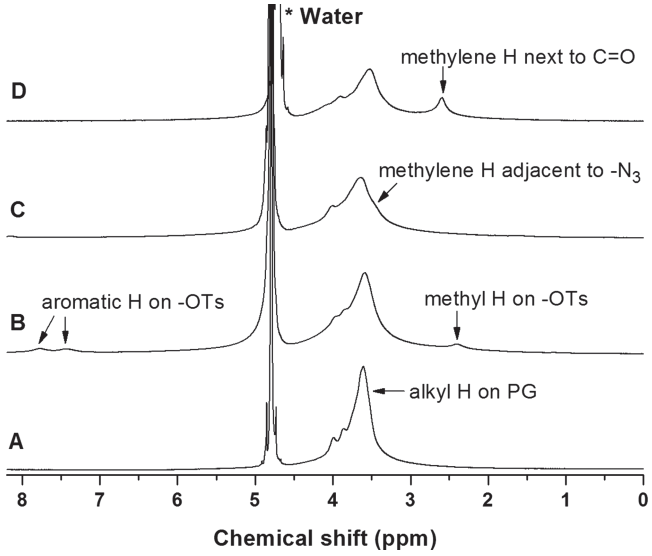

Figure 2. ^{1}H NMR spectra of A) ND50-PG, B) ND-PG-OTs, C) ND-PG-N_3 and D) ND-PG-N_3-COOH in D_2O.

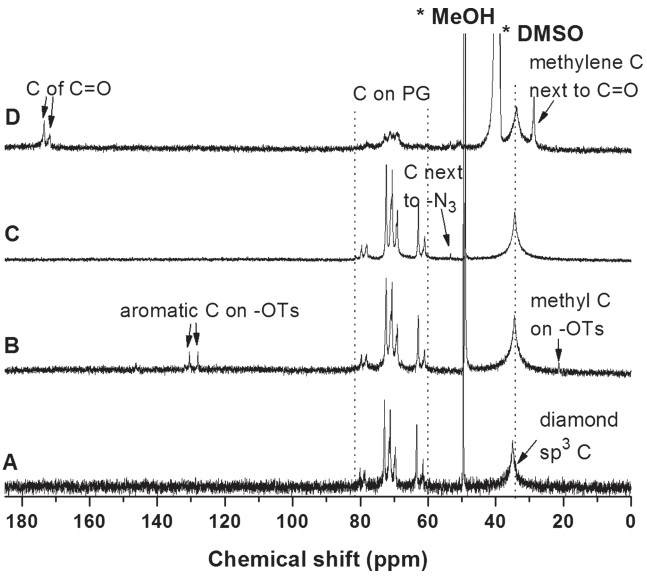

Figure 3. ^{13}C NMR spectra of A) ND50-PG, B) ND-PG-OTs and C) ND-PG-N_3 in D_2O, and D) ND-PG-N_3-COOH in DMSO-d_6.

through ring-opening of succinic anhydride are confirmed by a characteristic peak at 2.6 ppm, which is attributed to the methylene hydrogens next to carbonyl groups in ND-PG-N_3-COOH.

^{13}C NMR spectra (**Figure 3**) fully support the characterization of the ND50-PG derivatives by ^{1}H-NMR spectra mentioned above. In addition, ^{13}C NMR spectra provide the direct evidence of the existence of ND core;[63] that is, the characteristic sp^3 carbon signal of the diamond core was clearly distinguished at 35 ppm in all the ^{13}C NMR spectra shown in Figure 3. In Figure 3B, two kinds of the aromatic carbons and the methyl carbon at the tosyl groups in ND-PG-OTs are detected at 130 and 127 ppm, and 21 ppm, respectively. In the case of ND-PG-N_3 (Figure 3C), the signal at 53 ppm is assigned to the methylene carbons adjacent to azido groups. In Figure 3D, the carbons next to carbonyl groups are found at 29 ppm, and the carbonyl carbons at ester and carboxylic acid are clearly detected at 172 and 173 ppm. However, decent NMR spectra of ND-PG-RGD-COOH and ND-PG-RGD-Pt were not obtained, because the conjugation with RGD peptide decreased the solubility of the derivatives.

Although the aqueous solubility of ND-PG-Pt and ND-PG-RGD-Pt was not sufficient for NMR analysis, they can be readily dispersed in water and Dulbecco's modified Eagle's medium (DMEM) with concentration of >1.0 mg/mL. The aqueous solutions of ND-PG-Pt and ND-PG-RGD-Pt showed a narrow size distribution with hydrodynamic diameters of 59.5 ± 14.9 nm and 64.1 ± 15.0 nm, respectively. The content of platinum in ND-PG-Pt and ND-PG-RGD-Pt were estimated up to 17% and 14%, respectively, based on the measurement of inductively coupled plasma with atomic emission spectroscopy (ICP-AES).

2.2. Preparation and Characterization of Surface Functionalized Fluorescent ND (fND)

The intrinsic fluorescence of ND provides an ideal tool for cell labeling and intracellular tracking. In order to confirm cellular

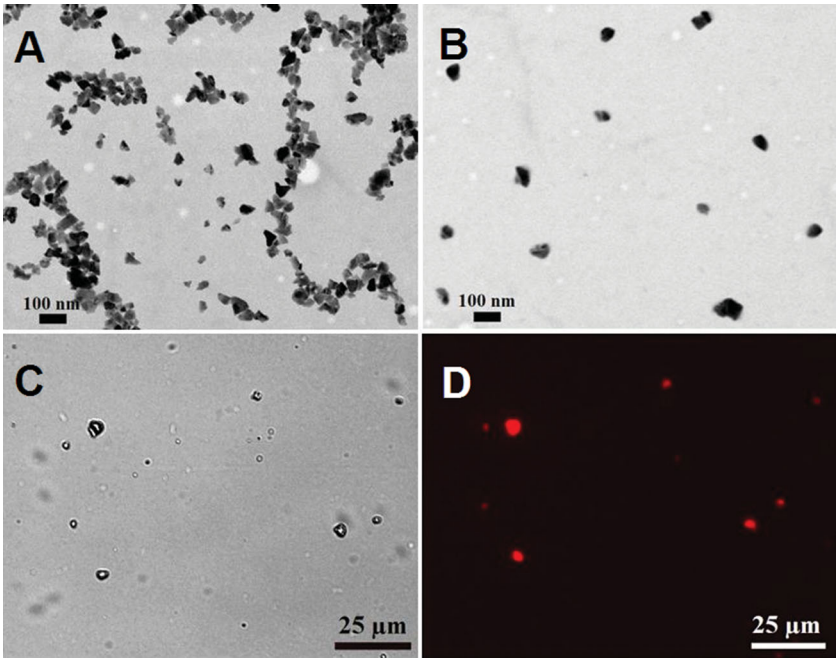

Figure 4. STEM images of A) fND and B) fND-PG, C) bright-field image of fND powder, and D) fluorescence image under cy3 mode.

uptake and intracellular localization of ND-PG and its derivatives, PG-functionalized fND and its derivatives were prepared in the same process shown in Scheme 1. ND50 was first air-oxidized to remove graphitic layer, then irradiated with helium ions and annealed to generate fluorescent nitrogen-vacancy (N-V) centers according to the method reported by Chang et al. (Supporting Information).[46] Since annealing process removes most of the oxygen containing functional groups and graphitizes the fND surface, air oxidization and mixed acid treatment were employed to regenerate the oxygen containing functional groups,[64,65] which can initiate the ring-opening polymerization of glycidol.[24]

As-prepared fND was characterized by scanning transmission electron microscopy (STEM), photoluminescence (PL) spectroscopy and fluorescence microscopy. The core of fND was clearly observed by STEM with a mean diameter of 48.2 ± 13.4 nm (**Figure 4**A). Upon excitation with 488-nm laser, the intrinsic emission of fND powder was detected at 550–800 nm using a PL spectrophotometer (Figure S1).[45] Fluorescence microscopy (Figure 4D) showed bright red fluorescence from the fND clusters which appear as gloomy dots in bright-field image (Figure 4C).

The as-prepared fND was functionalized by PG using the same method as that of ND50 mentioned above (Supporting Information).[24,34] However, when fND was sonicated in glycidol before polymerization, a large amount of precipitate was observed even after sonication for two hours. Actually, dynamic light scattering (DLS) measurements in water showed that fND includes large aggregates; its mean size (128 ± 50 nm) is 2.4 times larger than that of ND50 (52.8 ± 20.2 nm). The aggregation reduced specific surface area of fND for PG functionalization, leading to five times less aqueous solubility (4.0 mg/mL) than that of ND50-PG (≥20.0 mg/mL). In addition, the dispersion was not stable; precipitates were observed just after standing overnight.

To increase the aqueous solubility and stability, the second PG functionalization was employed to grow further the PG layer on the fND surface. The same procedure was employed as that of the first PG functionalization. The synthesized fND-PG was characterized by STEM, DLS, thermogravimetric analysis (TGA), and elemental analysis. STEM clearly shows deaggregation of fND after PG grafting twice (Figure 4B) with no significant change in the fND core size (**Table 1**). The deaggregation is supported by the reduction in the mean hydrodynamic diameter from fND (128 ± 50 nm) to fND-PG (63.4 ± 14.9 nm) determined by DLS (Table 1). As compared with ND50-PG, fND-PG has quite similar thickness in the PG layer and weight ratio in PG:ND; that is, the thickness calculated by the hydrodynamic and core sizes is 7.5 nm in fND-PG and 7.1 nm in ND50-PG (Table 1), and the weight ratio determined by TGA is 39:61 in fND-PG and 37:63 in ND50-PG (Figure S2). As expected, fND-PG displayed similar solubility to that of ND50-PG. Actual solubility of fND-PG in water, PBS and DMEM is ≥ 20, 15 and 12 mg/mL, respectively. These fND-PG solutions showed adequate stability; only a few precipitates were found over 3 months.

The result of the elemental analysis enables quantitative discussion of ND50-PG and fND-PG (**Table 2**). If the number of the carbon atoms consisting of ND50 and fND is assumed to be 1.2×10^7 calculated from the reported equation,[66] the numbers of the hydrogen and oxygen atoms in ND50 and fND are determined as shown in Table 2, based on the weight% of these elements in the elemental analysis. In addition, the ratio in atom numbers of C:H:O in ND50-PG and fND-PG is determined to be 6.22:3.76:1.37 and 6.04 : 3.65 : 1.39, respectively, from the results of the elemental analysis. Since PG layer, $(C_3H_6O_2)_n$, is added to ND50 and fND through ring-opening polymerization of glycidol ($C_3H_6O_2$), the above C:H:O ratios in ND50-PG and fND-PG correspond to $(1.2 \times 10^7 + 3n) : (1.3 \times 10^6 + 6n) : (3.8 \times 10^5 + 2n)$ and $(1.2 \times 10^7 + 3n) : (2.1 \times 10^6 + 6n) : (3.7 \times 10^5 + 2n)$, respectively. The degree of the ring-opening polymarization n is

Table 1. Size characterization of ND50, fND and their derivatives by STEM and DLS.

Particle	Core size [nm][a)]	Hydrodynamic size [nm] in water[b)]	Thickness of PG layer [nm][c)]
ND50	52.2 ± 14.4	52.8 ± 20.2	—
ND50-PG	52.7 ± 13.9	66.9 ± 14.8	7.1
fND	48.2 ± 13.4	128.4 ± 49.8	—
fND-PG	48.4 ± 12.8	63.4 ± 14.9	7.5

[a)]Average core diameter ± SD is determined by more than 100 particles in the STEM images; [b)]Mean diameter ± SD is determined by DLS on the basis of number distribution; [c)]Calculated from the difference of core size and hydrodynamic diameter.

Table 2. Elemental analysis of ND50 and fND before and after PG functionalization, and the estimated number of atoms consisting of each material.[a)]

Particle	C		H		O	
	[wt%]	number[b)]	[wt%]	number[b)]	[wt%]	number[b)]
ND50	94.89	1.2×10^7	0.89	1.3×10^6	3.99	3.8×10^5
ND50-PG	74.68	1.7×10^7	3.80	1.0×10^7	21.96	3.8×10^6
fND	91.46	1.2×10^7	1.37	2.1×10^6	3.72	3.7×10^5
fND-PG	72.57	1.7×10^7	3.89	1.1×10^7	22.27	4.0×10^6

[a)]Nitrogen is omitted because of low content (≤ 0.21%). CHN and O were measured independently by CHN and O modes. [b)]Number of atoms is calculated based on number of carbon atom (1.2×10^7) of a spherical ND with 50 nm size.[66]

calculated to be 1.7×10^6 and 1.8×10^6 for ND50-PG and fND-PG, respectively. Finally, the numbers of the carbon, hydrogen, and oxygen atoms in ND50-PG and fND-PG are determined as shown in Table 2 from the degree of polymarization n calculated above. Similar polymerization degrees in ND50-PG and fND-PG are supported by the similarity in these structural and physical properties mentioned above; hydrodynamic size, thickness in PG layer and aqueous solubility.

The fND-PG was further functionalized by the RGD peptide to confirm the selective uptake in the targeted tumor cell fluorescently, which will be mentioned below. The synthetic route is the same as that of ND50-PG shown in Scheme 1 (-OH → -OTs (tosylate) → -N_3 → -RGD). The resulting fND-PG-RGD exhibited good solubility and stability in water and DMEM (>1.0 mg/mL).

2.3. Biocompatibility, Cell Uptake, and Intracellular Localization of fND and Derivatives

Since biocompatibility is a prerequisite as drug delivery device, influence of fND, fND-PG and fND-PG-RGD on the viability of U87MG and HeLa cells was investigated. Dispersion or suspension of all three materials in DMEM exhibited no significant toxicity at concentrations up to 400 μg/mL to both types of cells for 24 h (Figure S4).

Next, cellular uptake of these materials was quantitatively compared using flow cytometry (FACS), after separately grown U87MG and HeLa cells were treated with fND, fND-PG and fND-PG-RGD at concentrations up to 200 μg/mL for 24 h (**Figure 5**). When FACS was performed, the parameter of side scattering (SSC) was measured at the same time with the red fluorescence (Figure 5 and S6). As a result, fND was taken up by both U87MG and HeLa in a concentration-dependent manner. In sharp contrast, neither U87MG nor HeLa displayed any significant fND-PG uptake even at the highest concentration, indicating stealth effect of the PG coating. In the case of fND-PG-RGD, however, U87MG and HeLa behaved differently. fND-PG-RGD uptake was dose-dependent in U87MG, but was not observed in HeLa even at the maximal concentration. In addition, change in the intensity of SSC (Figure 5B and D) exhibited a similar trend to that of red fluorescence (Figure 5A and C), suggesting that SSC signal is also an appropriate indicator of cellular incorporation of the ND-based materials.

The following conclusions can be drawn from the above results; 1) PG coating has shielding effect against cell uptake

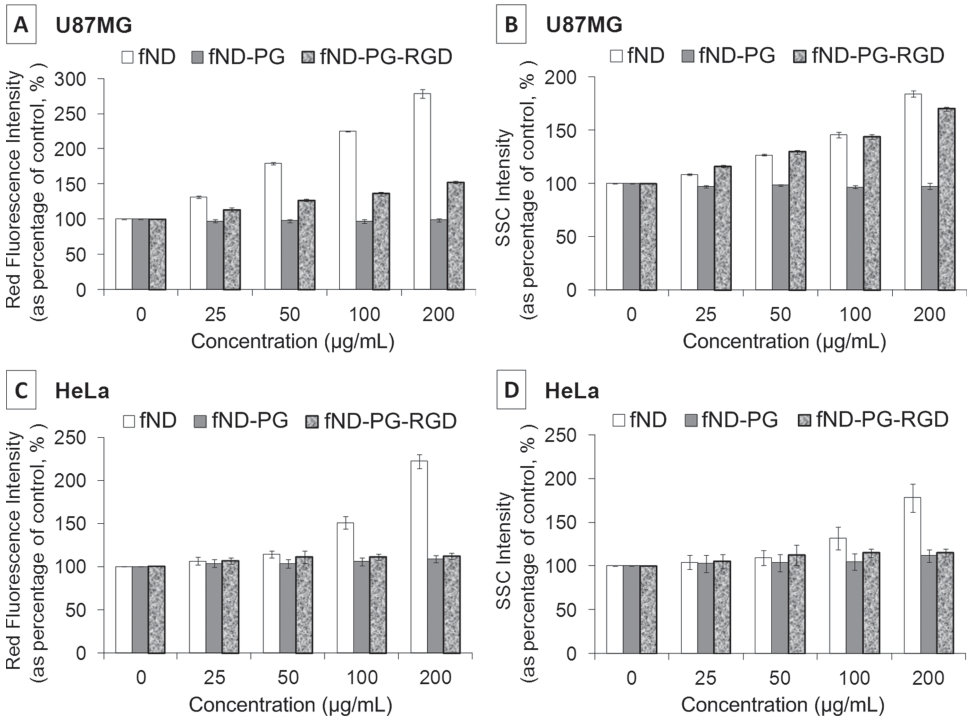

Figure 5. FACS analysis of uptake of fND, fND-PG and fND-PG-RGD in separately cultured U87MG and HeLa cells after 24-h treatment. Red fluorescence and side scattering (SSC) intensity were measured. Data were acquired on arithmetic scale and arithmetic means were used for quantification. Values are means ± SD ($n = 3$).

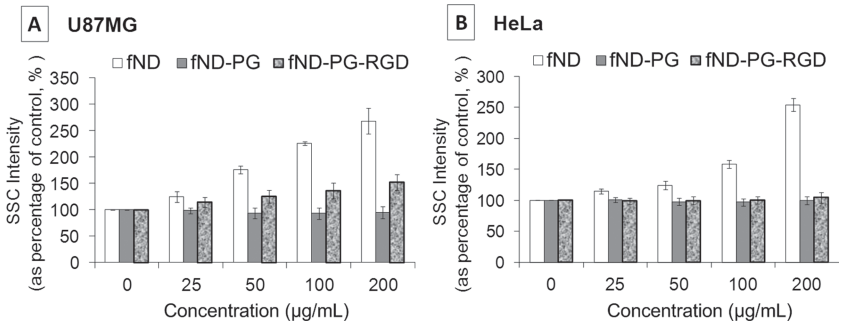

Figure 6. FACS analysis of uptake of fND, fND-PG and fND-PG-RGD in co-cultured U87MG and HeLa cells after 24-h treatment. Side scattering (SSC) intensity was measured. Data were acquired on arithmetic scale and arithmetic means were used for quantification. Values are means ± SD ($n = 6$).

and 2) RGD exerts targeting effect. To mimic the in vivo environment better, we grew U87MG and HeLa in mixed culture. U87MG cells were first labeled with 5(6)-carboxyfluorescein diacetate succinimidyl ester (CFDA-SE), a green fluorescent supravital dye for cell tracking, and then grown together with HeLa cells. After treatment of fND, fND-PG and fND-PG-RGD at concentrations up to 200 μg/mL for 24 h, the cells in the mixed culture were analyzed by FACS for uptake of the fND-based materials. Upon FACS, gating was set up so that U87MG cells were differentiated from HeLa cells by CFDA-SE fluorescence. Since the red fluorescence of fND cannot be used because of the strong green fluorescence from CFDA-SE, SSC signal was used for evaluation of cellular incorporation instead of the red fluorescence. The results obtained in the experiments using mixed culture (**Figure 6**) are consistent with those in the separate culture (Figure 5) mentioned above; extensive uptake of fND and very little uptake of fND-PG in both U87MG and HeLa cells, and selective uptake of fND-PG-RGD only in U87MG (Figure S6). The results obtained by FACS were also supported by fluorescent microphotographs (**Figure 7**). While cytoplasmically punctuated red fluorescence of the internalized fND was observed in both U87MG and HeLa treated with 200 μg/mL of fND (Figure 7B), neither type of the cell treated with fND-PG showed such clear red fluorescence at the same concentration (Figure 7C). When the co-culture was treated with 200 μg/mL of fND-PG-RGD, red fluorescence was observed only in the cytoplasm of U87MG cells, but not in HeLa (Figure 7D).

The lysosomal compartment is commonly reported as a major intracellular depositing site for internalized particles[51,67] and we confirmed fND-PG-RGD localized in the lysosomes by fluorescence microscopy. The lysosome of control U87MG cells were stained with LysoTracker Blue (Invitrogen) against mitochondrial counterstaining by rhodamine 123 (**Figure 8**A). LysoTracker Blue staining was then performed on U87MG cells treated with 200 μg/mL of fND-PG-RGD for 24 h. As shown in Figure 8B, the red fluorescence of the internalized fND-PG-RGD is found to co-localize with the blue staining of lysosomes.

2.4. Acid-Responsive Drug Release

In addition to the stealth effect of PG and targeting effect of RGD peptide, acid-responsive release of Pt(II) was confirmed in vitro as shown in Figure 8C.[68] The concentration of Pt liberated from the ND-PG-Pt was monitored by ICP-AES at 37 °C in the phosphate buffer solutions at the pH of 5.0 and 7.4. The initial Pt release rates from ND-PG-Pt are determined to be 57 μg/h and 30 μg/h at the pH of 5.0 and 7.4, respectively (Table S1). In the later stage (12–98 h), the Pt release rates are found to follow the first order kinetics and the rate constants are determined to be 2.9×10^{-3} and 1.7×10^{-3} h^{-1} at the pH of 5.0 and 7.4, respectively (Figure S3). That is, Pt release from ND-PG-Pt at the pH of lysosome (5.0) is almost two times faster than that at the pH of the cell culture medium (7.4), indicating the acid-responsive Pt release.

From the mechanistic point of view, we can interpret the acceleration of the Pt release reaction under acidic conditions as shown in **Scheme 2**, while the mechanism of the acid-responsive Pt release has been poorly documented.[43,68–70] The Pt(II) in the ND-PG-Pt forms square-planar structure.[71] Since the

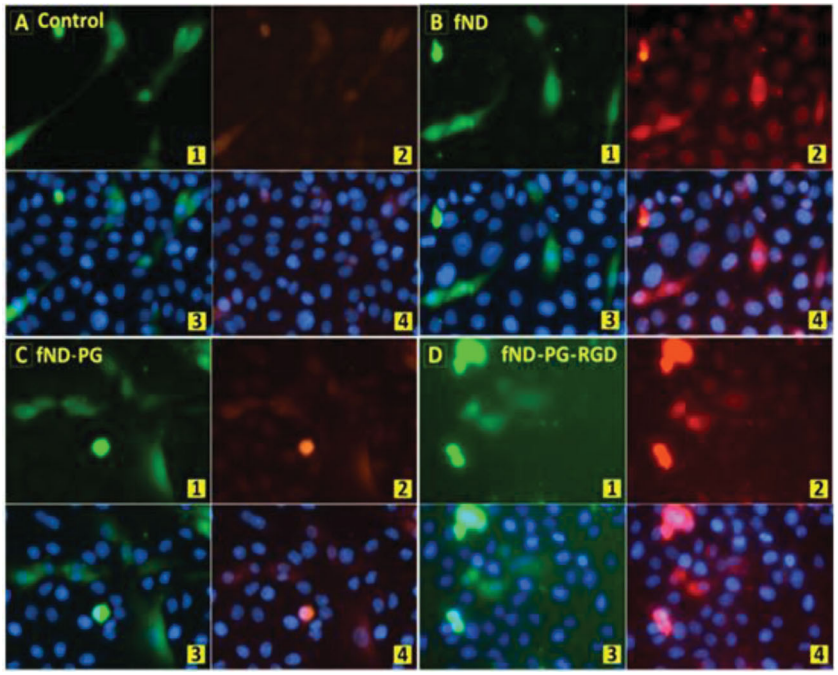

Figure 7. Fluorescent microphotographs of co-cultured U87MG and HeLa cells after 24-h treatment of fND, fND-PG and fND-PG-RGD (200 μg/mL). Three images of the same field were taken using different filters. 1 and 3: Green fluorescence was from U87MG stained with CFDA-SE. 2 and 4: Punctuated red fluorescence was from internalized fluorescent ND particles. 3 and 4: Blue fluorescence was from the nuclei of both U87MG and HeLa cells.

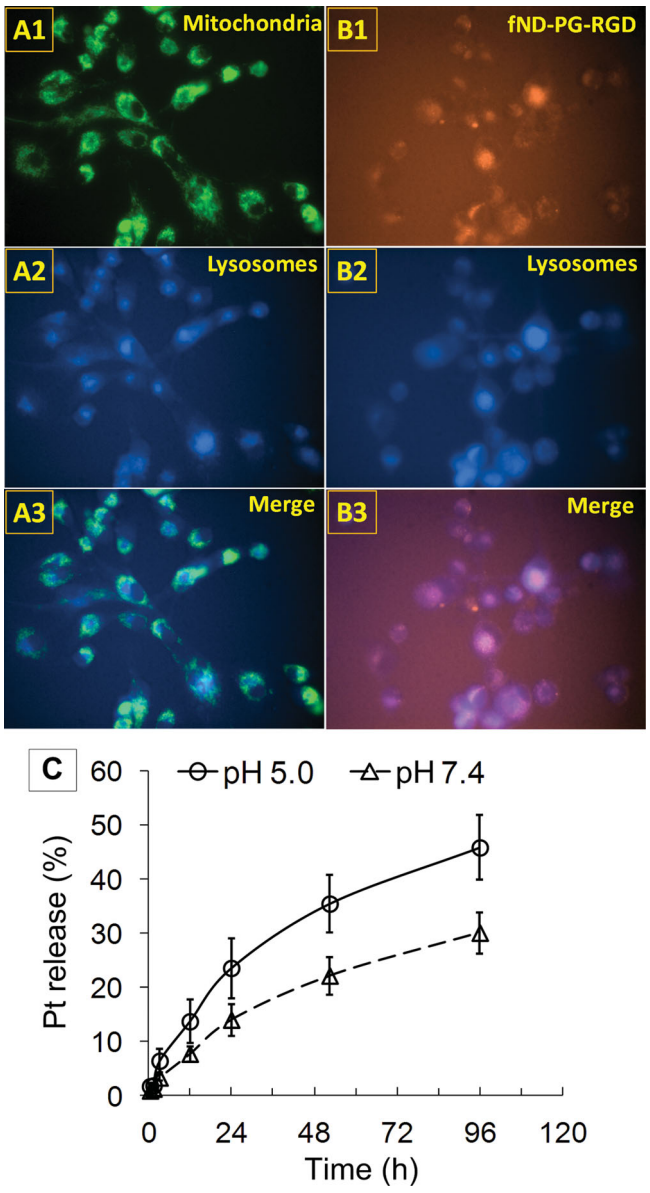

Figure 8. A and B: Subcellular localization of internalized fND-PG-RGD in U87MG cells. A1 and A2: Lysosomal staining by LysoTracker Blue with counter staining of mitochondria by rhodamine 123 in control cells. A3: A1 merged with A2. B1: Fluorescence of internalized fND-PG-RGD. B2: Lysosomal staining by LysoTracker Blue. B3: B1 merged with B2. C: Time course of platinum concentration released from ND-PG-Pt at pH of 5.0 and 7.4 ($n = 3$).

platinum-oxygen bonds are relatively labile compared with the very stable platinum-nitrogen ones, two carboxylates (COO^-) on Pt are considered to be substituted by water molecules to liberate *cis*-$[Pt(NH_3)_2(H_2O)_2]^{2+}$, *cis*-$[Pt(OH)(NH_3)_2(H_2O)]^+$ and/or *cis*-$[Pt(OH)_2(NH_3)_2]$ known as the cytotoxic forms of the cisplatin.[72–74] According to the literatures well documenting the ligand substitution process on the square planar Pt(II),[75] the Pt release from ND-PG-Pt is considered to proceed by the associative (S_N2 like) mechanism via trigonal bipyramidal intermediates (Scheme 2). Since the protonation at the carbonyl group makes the carboxylate better leaving group, acidic conditions are favored for the ligand substitution. Actually, the hydrogen ion concentration at pH 5.0 is 250 times larger than that at pH 7.4, hence accelerating the Pt release from the ND-PG-Pt prodrug as shown in Figure 8c.

The proposed mechanism of the acid-responsive Pt-drug release from the prodrug is considered to be applicable to the other Pt-based drugs with carboxylate and alkoxide ligands such as carboplatin, oxaliplatin and nedaplatin. These prodrugs are reported to reduce the dose limiting toxicity by slowing down the substitution of the carboxylate and alkoxide ligands with water molecules.[72] That is, they are more resistive to aquation than cisplatin at pH 7.4, reducing the side effects such as renal and nervous system toxicity. Under acidic conditions in tumor cells, however, the aquation is considered to be accelerated to release actual drug, which can form adducts with DNA, according to the proposed mechanism shown in Scheme 2.

2.5. In Vitro Drug Delivery and Cytotoxicity Assay

Subsequently to the drug release, the drug efficacy was compared among the Pt(II)-based prodrugs with and without stealth PG and targeting peptide. Separately grown U87MG and HeLa cells were treated with cisplatin, ND-PG-Pt and ND-PG-RGD-Pt for 24 h at the platinum concentrations of 0–20 μg/mL as shown in **Figure 9**A and B. Cisplatin was toxic to both U87MG and HeLa, while ND-PG-Pt was almost non-toxic to both cells. ND-PG-RGD-Pt exhibited little toxicity in HeLa (Figure 9B), but similar toxicity to cisplatin in U87MG (Figure 9A). Microphotographs also provided direct visual evidence (Figure S7). The non-toxicity of ND-PG-Pt to both cells and the selective toxicity of ND-PG-RGD-Pt to U87MG are well correlated with the cellular uptake behavior of fND-PG and fND-PG-RGD mentioned above (Figures 5–7). Platinum levels inside the U87MG and HeLa cells were quantified after 24-hour treatment of cisplatin, ND-PG-Pt and ND-PG-RGD-Pt (Figure 9C). As a result, platinum contents in both types of cells were highest in the cisplatin treatment and lowest in the ND-PG-Pt treatment. While ND-PG-RGD-Pt exhibited only slightly higher platinum level than ND-PG-Pt in the HeLa cells, the platinum level in U87MG cells treated by ND-PG-RGD-Pt is significantly higher than that treated by ND-PG-Pt and is close to that of the cisplatin-treated cells. We can conclude that PG surface coating provides stealth effect so that ND-PG-Pt avoids non-specific cell uptake and lacks cytotoxicity. On this basis, ND-PG-RGD-Pt only enters into U87MG, but not HeLa, by virtue of RGD targeting and releases the loaded platinum-based drug to exert selective cytotoxicity.

3. Conclusion

Through rational surface engineering based on synthetic organic chemistry, targeting RGD peptide and anticancer drug were immobilized on the ND-PG platform. PG layer endowed ND-PG and its derivatives with good solubility in aqueous media, enabling more precise characterization by solution phase NMRs. In addition, PG shielded ND from non-specific cell uptake. ND-PG conjugated with the RGD peptide (ND-PG-RGD) was taken up by U87MG, but not HeLa cell. When the

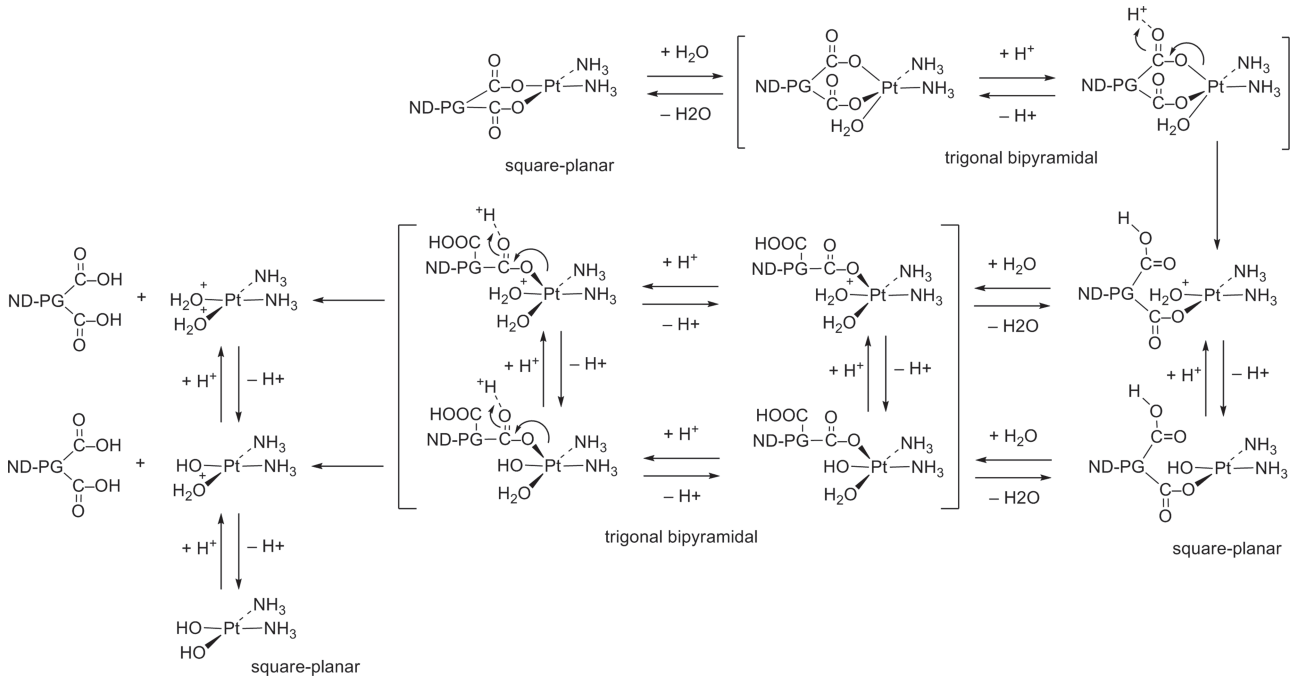

Scheme 2. Plausible ligand substitution mechanism on the acid-responsive release of Pt(II) drug from the ND-PG-Pt prodrug.

platinum-based anticancer drug was loaded, ND-PG-Pt avoided non-specific cell uptake due to the stealth effect of PG and hence exhibited no cytotoxicity to both U87MG and HeLa cells. In sharp contrast, ND-PG-RGD-Pt demonstrated cytotoxicity only to U87MG cell by virtue of the targeting effect of RGD as well as the stealth effect of PG.

The methodology to prepare ND-PG-RGD-Pt, described so far, has a wide scope to construct the multi-functional nanoparticle for in vivo application, because one can simply replace the pieces in accordance with the purpose. For any target, the targeting peptide can be identified by phage display method[76] and immobilized on the PG layer through click chemistry in place of the RGD peptide. In addition, the core material can be replaced by various nanoparticles by virtue of the generality in the PG fuctionalization.[24–26,41] The size can be tuned in view of passive targeting of the tumor lesion.[24,77] The drugs other than Pt-based one can be also loaded on the PG-coated nanoparticle backbone through not only coordination bonding but also covalent and hydrogen bonding. We believe that the flexibility and versatility in the design and construction of the PG-based prodrugs can make significant progress on the in vivo application of the nanoparticles in the field of nanomedicine.

4. Experimental Section

Synthesis and Characterization of ND50-PG: ND50-PG was prepared according to our reported method,[24] using ND50 as a starting material and characterized by FTIR (Figure 1A), and solution-phase ^{1}H- and ^{13}C-NMR (Figure 2A and 3A).

Synthesis and Characterization of ND-PG-OTs: ND50-PG (100 mg) was dissolved in pyridine (4.0 mL) by bath sonication and then cooled down to 0 °C in an ice/water bath. *p*-Toluenesulfonyl chloride (200 mg, 1.05 mmol) was dissolved in pyridine (2.0 mL) and added dropwise into the mixture under rapid stirring. The solution was stirred at 0–5 °C for 3 h and at room temperature overnight. The resulting solid was collected by centrifugation (Avanti J-E, Beckman Coulter) at 50400*g* and purified in DMF by repeated redispersion/centrifugation cycles. It was characterized by FTIR (Figure 1B), and solution-phase ^{1}H- and ^{13}C-NMR (Figure 2B and 3B).

Synthesis and Characterization of ND-PG-N$_3$: Sodium azide (100 mg, 1.54 mmol) in water (2.0 mL) was added into ND-PG-OTs (80 mg) in DMF (6.0 mL) and stirred at 90 °C overnight. After cooling down, the product was collected by centrifugation and purified in water by repeated redispersion/centrifugation cycles. It was characterized by FTIR (Figure 1C), and solution-phase ^{1}H- and ^{13}C-NMR (Figure 2C and 3C).

Synthesis and Characterization of ND-PG-N$_3$-COOH: ND-PG-N$_3$ (50 mg) and 4-dimethylaminopyridine (1.5 mg) was dissolved in pyridine (4.0 mL) by bath sonication and then cooled down to 0 °C in an ice bath. Succinic anhydride (40 mg, 0.40 mmol) was dissolved in pyridine (2.0 mL) and added dropwise into the mixture under rapid stirring. The solution was stirred at 0–5 °C for 3 h and at room temperature overnight. The resulting solid was collected by centrifugation and purified in DMF by repeated redispersion/centrifugation cycles. It was characterized by FTIR (Figure 1D), and solution-phase ^{1}H- and ^{13}C-NMR (Figure 2D and 3D).

Synthesis and Characterization of ND-PG-RGD-COOH: RGD propargyl amide[25] (4.0 mg) in water (1.0 mL) was added to a solution of ND-PG-N$_3$-COOH (20 mg) in water (2.0 mL). Copper(II) sulfate pentahydrate (8 mg) in water (0.5 mL) and sodium ascorbate (10 mg) in water (0.5 mL) were added into the mixture with vigorous stirring. The resulting brown suspension was bath sonicated for 10 min and stirred at room temperature for 48 h. Diluted ammonia was dropped into the suspension to dissolve insoluble copper salts, giving a clear blue-gray solution. The solid was collected by high-speed centrifugation and purified in 1% ammonia by repeated washing/centrifugation. It was characterized by FTIR (Figure 1E).

Synthesis and Characterization of ND-PG-RGD-Pt: ND-PG-RGD-COOH (20 mg) and cisplatin (4.8 mg, 0.016 mmol) were mixed in Milli-Q water (4.0 mL) by bath sonication. The pH of the mixture was adjusted to 8.0 using 0.5 M NaOH. After stirring at room temperature in dark for 72 h, the mixture was passed through a 0.45-μm cellulose filter (Millipore) to remove insoluble solid. The unbound cisplatin in filtrate was removed

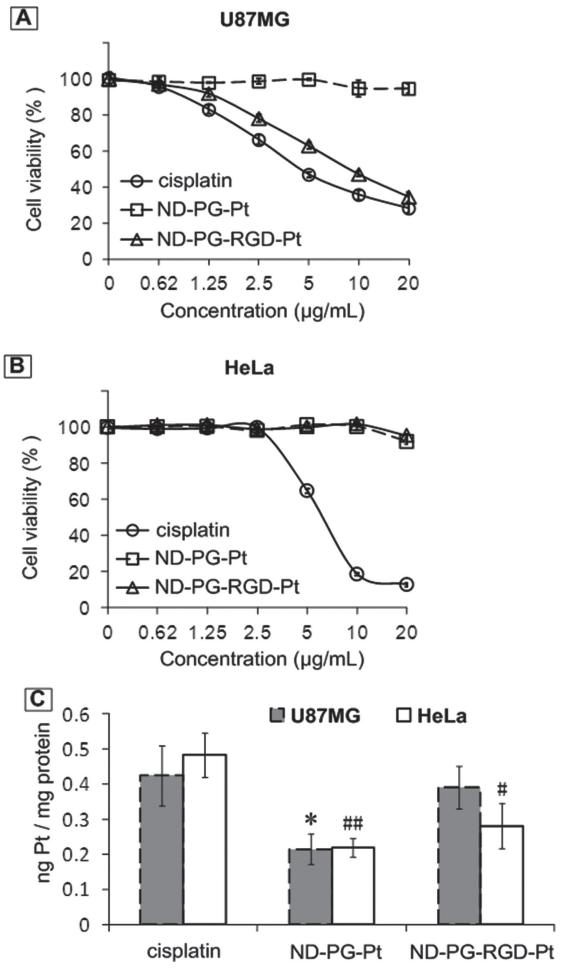

Figure 9. A and B: Cell killing effect of cisplatin, ND-PG-Pt and ND-PG-RGD-Pt. Concentrations were normalized to platinum up to 20 μg/mL. Treatment duration was 24 h (n = 3). C: Platinum levels (normalized to protein concentrations) in U87MG and HeLa cells after 24-h treatment of cisplatin, ND-PG-Pt and ND-PG-RGD-Pt containing 2.5 μg/mL of platinum. Values are means ± SD (n = 3). Student's t-test was performed (* and # $p < 0.05$, ## $p < 0.01$).

by the dialysis in 200 mL of Milli-Q water and the medium was changed every 4 h for 3 times. For cell experiments, the purified sample was further dialyzed against DMEM to replace the medium to a physiological solution. It was characterized by FTIR (Figure 1F).

Supporting Information

Supporting Information is available from the Wiley Online Library or from the author. It includes Figures S1 and S2, materials and instruments, method of solubility measurement, preparation of fND and fND-PG, and experimental details of the in vitro drug release (Table S1 and Figure S3) and in vitro cell experiments (Figures S4–S7).

Acknowledgements

This work was financially supported by Science and Technology Incubation Program in Advanced Region (JST), Industrial Technology Research Grant Program (NEDO), Grant-in-Aid for Challenging Exploratory Research (JSPS), and Grants-in-Aid for Scientific Research (NO. 2400210802) (JSPS). X. C. thanks the JSPS for providing the Postdoctoral Fellowship (NO. P12108). The authors thank Tomei Diamond Co., Ltd. for providing us with ND50.

Received: December 28, 2013
Revised: March 14, 2014
Published online: May 23, 2014

[1] K. Riehemann, S. W. Schneider, T. A. Luger, B. Godin, M. Ferrari, H. Fuchs, *Angew. Chem. Int. Ed.* **2009**, *48*, 872.
[2] Y. Liu, H. Miyoshi, M. Nakamura, *Int. J. Cancer* **2007**, *120*, 2527.
[3] S. D. Caruthers, S. A. Wickline, G. M. Lanza, *Curr. Opin. Biotechnol.* **2007**, *18*, 26.
[4] V. Wagner, A. Dullaart, A.-K. Bock, A. Zweck, *Nat. Biotechnol.* **2006**, *24*, 1211.
[5] K. K. Jain, *Clin. Chim. Acta* **2005**, *358*, 37.
[6] C. Minelli, S. B. Lowe, M. M. Stevens, *Small* **2010**, *6*, 2336.
[7] M. Baker, *Nat. Methods* **2010**, *7*, 957.
[8] O. C. Farokhzad, R. Langer, *ACS Nano* **2009**, *3*, 16.
[9] M. De, P. S. Ghosh, V. M. Rotello, *Adv. Mater.* **2008**, *20*, 4225.
[10] J. Rao, *ACS Nano* **2008**, *2*, 1984.
[11] K. B. Hartman, L. J. Wilson, M. G. Rosenblum, *Mol. Diagn. Ther.* **2008**, *12*, 1.
[12] D. Peer, J. M. Karp, S. Hong, O. C. Farokhzad, R. Margalit, R. Langer, *Nat. Nanotechnol.* **2007**, *2*, 751.
[13] D. F. Emerich, C. G. Thanos, *J. Drug Target.* **2007**, *15*, 163.
[14] J. A. Barreto, W. O'Malley, M. Kubeil, B. Graham, H. Stephan, L. Spiccia, *Adv. Heathcare Mater.* **2011**, *23*, H18.
[15] E. Gullotti, Y. Yeo, *Mol. Pharmaceutics* **2009**, *6*, 1041.
[16] S.-D. Li, L. Huang, *Mol. Pharmaceutics* **2008**, *5*, 496.
[17] S. D. Perrault, C. Walkey, T. Jennings, H. C. Fischer, W. C. W. Chan, *Nano Lett.* **2009**, *9*, 1909.
[18] H. Maeda, *Bioconjugate Chem.* **2010**, *21*, 797.
[19] Z. Amoozgar, Y. Yeo, *Wiley Interdiscip. Rev. Nanomed. Nanobiotechnol.* **2012**, *4*, 219.
[20] A. Sunder, R. Hanselmann, H. Frey, R. Mülhaupt, *Macromolecules* **1999**, *32*, 4240.
[21] T. Takimoto, T. Chano, S. Shimizu, H. Okabe, M. Ito, M. Morita, T. Kimura, T. Inubushi, N. Komatsu, *Chem. Mater.* **2010**, *22*, 3462.
[22] M. Calderón, M. A. Quadir, S. K. Sharma, R. Haag, *Adv. Mater.* **2010**, *22*, 190.
[23] D. Wilms, S.-E. Stiriba, H. Frey, *Acc. Chem. Res.* **2010**, *43*, 129.
[24] L. Zhao, T. Takimoto, M. Ito, N. Kitagawa, T. Kimura, N. Komatsu, *Angew. Chem. Int. Ed.* **2011**, *50*, 1388.
[25] L. Zhao, T. Chano, S. Morikawa, Y. Saito, A. Shiino, S. Shimizu, T. Maeda, T. Irie, S. Aonuma, H. Okabe, T. Kimura, T. Inubushi, N. Komatsu, *Adv. Funct. Mater.* **2012**, *22*, 5107.
[26] L. Zhao, T. Takimoto, T. Kimura, N. Komatsu, *J. Indian Chem. Soc.* **2011**, *88*, 1787.
[27] R. K. Kainthan, J. Janzen, E. Levin, D. V. Devine, D. E. Brooks, *Biomacromolecules* **2006**, *7*, 703.
[28] R. K. Kainthan, S. R. Hester, E. Levin, D. V. Devine, D. E. Brooks, *Biomaterials* **2007**, *28*, 4581.
[29] M. Weinhart, I. Grunwald, M. Wyszogrodzka, L. Gaetjen, A. Hartwig, R. Haag, *Chem. Asian J.* **2010**, *5*, 1992.
[30] R. K. Kainthan, D. E. Brooks, *Biomaterials* **2007**, *28*, 4779.
[31] L. Wang, K. G. Neoh, E. T. Kang, B. Shuter, S.-C. Wang, *Adv. Funct. Mater.* **2009**, *19*, 2615.
[32] N. Arsalani, H. Fattahi, S. Laurent, C. Burtea, L. V. Elst, R. N. Muller, *Contrast Media Mol. Imaging* **2012**, *7*, 185.
[33] L. Wang, K. G. Neoh, E.-T. Kang, B. Shuter, *Biomaterials* **2011**, *32*, 2166.

[34] J.-P. Boudou, M.-O. David, V. Joshi, H. Eidi, P. A. Curmi, *Diamond Relat. Mater.* **2013**, *38*, 131.
[35] L. Zhao, Y. Nakae, H. Qin, T. Ito, T. Kimura, H. Kojima, L. Chan, N. Komatsu, *Beilstein J. Org. Chem.* **2014**, *10*, 707.
[36] L. Zhao, A. Shiino, H. Qin, T. Kimura, N. Komatsu, *J. Nanosci. Nanotechnol.* 2014, DOI:10.1166/jnn.2014.9738.
[37] C. S. Popeney, A. Setaro, R.-C. Mutihac, P. Bluemmel, B. Trappmann, J. Vonneman, S. Reich, R. Haag, *ChemPhysChem* **2012**, *13*, 203.
[38] F. Ernst, T. Heek, A. Setaro, R. Haag, S. Reich, *Adv. Funct. Mater.* **2012**, *22*, 3921.
[39] A. Setaro, C. S. Popeney, B. Trappmann, R. Haag, S. Reich, *Phys. Status Solidi B* **2010**, *247*, 2758.
[40] L. Zhou, C. Gao, W. Xu, *Macromol. Chem. Phys.* **2009**, *210*, 1011.
[41] L. Zhou, C. Gao, W. Xu, X. Wang, Y. Xu, *Biomacromolecules* **2009**, *10*, 1865.
[42] T. Jafari, A. Simchi, N. Khakpash, *J. Colloid Interface Sci.* **2010**, *345*, 64.
[43] J. Gu, S. Su, Y. Li, Q. He, J. Zhong, J. Shi, *J. Phys. Chem. Lett.* **2010**, *1*, 3446.
[44] J. H. Jeong, J. J. Schmidt, R. E. Kohman, A. T. Zill, R. J. DeVolder, C. E. Smith, M.-H. Lai, A. Shkumatov, T. W. Jensen, L. G. Schook, S. C. Zimmerman, H. Kong, *J. Am. Chem. Soc.* **2013**, *135*, 8770.
[45] S.-J. Yu, M.-W. Kang, H.-C. Chang, K.-M. Chen, Y.-C. Yu, *J. Am. Chem. Soc.* **2005**, *127*, 17604.
[46] Y.-R. Chang, H.-Y. Lee, K. Chen, C.-C. Chang, D.-S. Tsai, C.-C. Fu, T.-S. Lim, Y.-K. Tzeng, C.-Y. Fang, C.-C. Han, H.-C. Chang, W. Fann, *Nat. Nanotechnol.* **2008**, *3*, 284.
[47] V. N. Mochalin, O. Shenderova, D. Ho, Y. Gogotsi, *Nat. Nanotechnol.* **2012**, *7*, 11.
[48] Y. Xing, L. Dai, *Nanomedicine* **2009**, *4*, 207.
[49] R. J. Narayan, R. D. Boehm, A. V. Sumant, *Mater. Today* **2011**, *14*, 154.
[50] C.-C. Fu, H.-Y. Lee, K. Chen, T.-S. Lim, H.-Y. Wu, P.-K. Lin, P.-K. Wei, P.-H. Tsao, H.-C. Chang, W. Fann, *Proc. Natl. Acad. Sci.* USA **2007**, *104*, 727.
[51] O. Faklaris, V. Joshi, T. Irinopoulou, P. Tauc, M. Sennour, H. Girard, C. Gesset, J.-C. Arnault, A. Thorel, J. P. Boudou, P. A. Curmi, F. Treussart, *ACS Nano* **2009**, *3*, 3955.
[52] N. Mohan, Y.-K. Tzeng, L. Yang, Y.-Y. Chen, Y. Y. Hui, C.-Y. Fang, H.-C. Chang, *Adv. Mater.* **2010**, *22*, 843.
[53] R. Martin, M. Alvaro, J. R. Herance, H. Garcia, *ACS Nano* **2010**, *4*, 65.
[54] Y. Li, X. Zhou, D. Wang, B. Yang, P. Yang, *J. Mater. Chem.* **2011**, *21*, 16406.
[55] E. K. Chow, X.-Q. Zhang, M. Chen, R. Lam, E. Robinson, H. Huang, D. Schaffer, E. Osawa, A. Goga, D. Ho, *Sci. Transl. Med.* **2011**, *3*, 73ra21.
[56] X.-Q. Zhang, M. Chen, R. Lam, X. Xu, E. Osawa, D. Ho, *ACS Nano* **2009**, *3*, 2609.
[57] X.-Q. Zhang, R. Lam, X. Xu, E. K. Chow, H.-J. Kim, D. Ho, *Adv. Mater.* **2011**, *23*, 4770.
[58] Y.-K. Tzeng, O. Faklaris, B.-M. Chang, Y. Kuo, J.-H. Hsu, H.-C. Chang, *Angew. Chem. Int. Ed.* **2011**, *50*, 2262.
[59] A. Bumb, S. K. Sarkar, N. Billington, M. W. Brechbiel, K. C. Neuman, *J. Am. Chem. Soc.* **2013**, *135*, 7815.
[60] H. Maeda, J. Wu, T. Sawa, Y. Matsumura, K. Hori, *J. Control. Release* **2000**, *65*, 271.
[61] L. Ye, K. Letchford, M. Heller, R. Liggins, D. Guan, J. N. Kizhakkedathu, D. E. Brooks, J. K. Jackson, H. M. Burt, *Biomacromolecules* **2010**, *12*, 145.
[62] Y. Zhang, H. He, C. Gao, *Macromolecules* **2008**, *41*, 9581.
[63] N. Komatsu, N. Kadota, T. Kimura, E. Osawa, *Chem. Lett.* **2007**, *36*398.
[64] S. Osswald, G. Yushin, V. Mochalin, S. O. Kucheyev, Y. Gototsi, *J. Am. Chem, Soc.* **2006**, *128*, 11635.
[65] J. Havlik, V. Petrakova, I. Rehor, V. Petrak, M. Gulka, J. Stursa, J. Kucka, J. Ralis, T. Rendler, S.-Y. Lee, R. Reuter, J. Wrachtrup, M. Ledvina, M. Nesladek, P. Cigler, *Nanoscale* **2013**, *5*, 3208.
[66] O. A. Shenderova, V. V. Zhirnov, D. W. Brenner, *Crit. Rev. Solid State Mater. Sci.* **2002**, *27*, 227.
[67] S. Manchun, C. R. Dass, P. Sriamornsak, *Life Sci.* **2012**, *90*, 381.
[68] B. Guan, F. Zou, J. Zhi, *Small* **2010**, *6*, 1514.
[69] P. Xu, E. A. Van Kirk, W. J. Murdoch, Y. Zhan, D. D. Isaak, M. Radosz, Y. Shen, *Biomacromolecules* **2006**, *7*, 829.
[70] S. Aryal, C.-M. J. Hu, L. Zhang, *ACS Nano* **2009**, *4*, 251.
[71] J. Reedijk, P. H. M. Lohman, *Pharm. Weekblad Sci. Ed.* **1985**, *7*, 173.
[72] K. J. Haxton, H. M. Burt, *J. Pharm. Sci.* **2009**, *98*, 2299.
[73] K. J. Haxton, H. M. Burt, *Dalton Trans.* **2008**, 5872.
[74] L. Z. Zwelling, K. W. Kohn, *Cancer Treat. Rep.* **1979**, *63*, 1439.
[75] C. H. Lamngford, H. B. Gray, *Ligand Substitution Processes*, W. A. Benjamin, Inc., New York **1966**.
[76] R. Giordano, M. Cardó-Vila, J. Lahdenranta, R. Pasqualini, W. Arap, *Nat. Med.* **2001**, *7*, 1249.
[77] Y. Morita, T. Takimoto, H. Yamanaka, K. Kumekawa, S. Morino, S. Aonuma, T. Kimura, N. Komatsu, *Small* **2008**, *4*, 2154.